Editors' Suggestion

Entanglement improvement via a quantum scissor in a realistic environment

Liyun Hu,[1,2,*] M. Al-amri,[1,3,4,5,†] Zeyang Liao,[1,6] and M. S. Zubairy[1,‡]

[1]*Institute for Quantum Science and Engineering (IQSE) and Department of Physics & Astronomy, Texas A&M University, College Station, Texas 77843, USA*

[2]*Center for Quantum Science and Technology, Jiangxi Normal University, Nanchang 330022, China*

[3]*CQOQI, KACST, Riyadh 11442, Saudi Arabia*

[4]*The National Center for Laser and Optoelectronics, KACST, Riyadh 11442, Saudi Arabia*

[5]*Department of Physics, KKU, P.O Box 9004, Abha 61413, Saudi Arabia*

[6]*School of Physics, Sun Yat-sen University, Guangzhou 510275, China*

(Received 8 August 2019; published 18 November 2019)

We propose a protocol for improving quantum entanglement based on a quantum scissor scheme [D. T. Pegg *et al.*, Phys. Rev. Lett. **81**, 1604 (1998)]. Compared to existing protocols for entanglement improvement, our scheme does not require biside operation on two-mode squeezed vacuum states. This greatly enhances the success probability as well as entanglement, while reducing the resources. A squared gain factor can be obtained from our scheme. In addition, our scheme is robust against the decoherence when considering more realistic cases. Finally, a comparison between the single-side quantum scissor scheme and the single-side quantum catalysis is also investigated.

DOI: 10.1103/PhysRevA.100.052322

I. INTRODUCTION

Quantum entanglement plays a central role in the fields of quantum information and quantum computation [1,2]. However, how to protect or enhance entanglement when it comes to realistic situations is still a challenging problem. The entanglement cannot be improved by local Gaussian unitary operation due to the limitation of the no-go theorem [3–5]. However, many schemes using local non-Gaussian operation are proposed theoretically and experimentally [6–25]. For example, the entanglement in the continuous-variable two-mode squeezed vacuum state (TMSVS) can be improved by applying photon addition and subtraction to one or both modes. Photon catalysis offers another scheme for the entanglement enhancement where non-Gaussian operations can be implemented using a photon number state as the input of a beam splitter. Quantum catalysis has been shown as a method to accomplish noiseless linear amplification (NLA) [26–28] and coherence enhancement [29], and to improve the performance of quantum key distribution [30]. All of these non-Gaussian operations, which can be implemented using the number state as the input of a beam splitter, are probabilistic. Thus, from the point of operation, the success probability of such events should be taken into account.

In this paper, we introduce a scheme based on the quantum scissor idea that not only improves entanglement but with less resources and higher success probability compared to the existing schemes. The enhancement of amplification is verified, using a single-side modified quantum scissor, for a single-mode coherent state and two-mode squeezed vacuum. We further propose a more realistic scenario by replacing the ideal single-photon state and photon detectors with the heralded single-photon state and on-off photon detectors. We show that an overall improvement can still be accomplished by single-side operation even when both modes of the TMSVS pass through the lossy channels.

This paper is organized as follows. In Sec. II, we introduce the modified quantum scissor model and derive analytically the general input-output relation using operator formalism for any input state. We demonstrate that a squared gain factor can be obtained for coherent-state input compared to the original scheme. In Sec. III, we apply a single-side and biside quantum scissor device to both one mode and two modes of the TMSVS, respectively. A comparison is made with respect to the entanglement enhancement and corresponding success probability. In Sec. IV, we further consider the realistic TMSVS and ideal quantum scissor device. In Sec. V, we discuss a more realistic scenario: a realistic quantum scissor device applied to a realistic TMSVS. We summarize our results in Sec. VI.

II. MODEL OF QUANTUM SCISSOR AND ITS CORRESPONDING OPERATOR

In this section, we first examine the quantum scissor from the operator point of view. As shown in Fig. 1, the quantum scissor device consists of two beam splitters (denoted as BS_{ac} and BS_{bc}) and two ideal single-photon detectors (denoted by D_1 and D_2). The transmission coefficients of the two beam splitters are T_{ac} and T_{bc}. The single-photon state $|1\rangle_b$ and vacuum state $|0\rangle_c$ are fed into the two input ports of an asymmetrical beam splitter (BS_{bc}) to generate an entangled state. Thus, the input mode a for the input state ρ_{in} is combined

*hlyun@jxnu.edu.cn
†mdalamri@kacst.edu.sa
‡zubairy@physics.tamu.edu

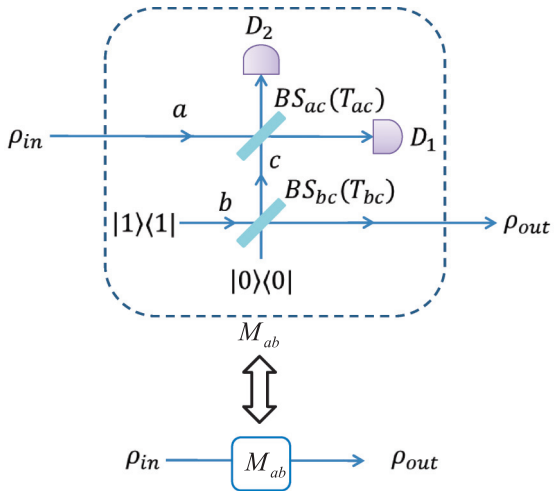

FIG. 1. Quantum scissors scheme for any input state $\rho_{\rm in}$. The effect will convert any input state into an output state in a Fock space spanned by both a vacuum and single photon. The beam splitters (BS_{ac} and BS_{bc}) are asymmetrical with transmission coefficient T_{ac} and T_{bc}, respectively. The relation between the output and input states can be described by an operator M_{ab}.

with mode c in the second asymmetrical BS_{ac} (T_{ac}). In the original scheme [26,31], the quantum scissor device consists of a symmetrical ($T_{ac} = 1/2$) and an asymmetrical (T_{bc}) beam splitter. The expected output state can be heralded successfully when two detectors D_1 and D_2 register (1,0) at modes a and c, respectively, since the output state is conditioned on the measurement results of the two detectors D_1 and D_2, which is in some sense similar to quantum teleportation. If the quantum scissor protocol is used for quantum teleportation in a distant place, a classical communication channel is needed. However, if it is used for quantum entanglement improvement in a local place, a classical communication channel is not needed.

For any pure input state $\rho_{\rm in} = |\psi\rangle_{\rm in,in}\langle\psi|$, the output state $|\psi\rangle_{\rm out}$ can be given by

$$|\psi\rangle_{\rm out} = \frac{1}{\sqrt{p_d}} M_{ab}|\psi\rangle_{\rm in}, \tag{1}$$

where p_d is the success probability of such an event, and M_{ab} is a kind of projective measurement corresponding to the quantum-scissor operation in the dashed box in Fig. 1, which is an operator for input mode a and final output mode b. Mathematically, M_{ab} can be represented as

$$M_{ab} = {}_c\langle 0|_a\langle 1|B_{ac}B_{bc}|1\rangle_b|0\rangle_c, \tag{2}$$

where $B_{kl} = \exp[\theta(a_k^\dagger a_l - a_l^\dagger a_k)]$ are the unitary operators coupling both k and l modes by a beam splitter, and the transmission coefficient $T_{kl} = \cos^2\theta$. Here, $a_k^\dagger(a_k)$ and $a_l^\dagger(a_l)$ are the creation (annihilation) operators for the k and l modes, respectively.

In order to see the operation of the quantum scissor device, we consider the following transformation relations [32]:

$$B_{kl}\begin{pmatrix} a_k \\ a_l \end{pmatrix} B_{kl}^\dagger = \begin{pmatrix} \sqrt{T_{kl}} & -\sqrt{R_{kl}} \\ \sqrt{R_{kl}} & \sqrt{T_{kl}} \end{pmatrix}\begin{pmatrix} a_k \\ a_l \end{pmatrix}, \tag{3}$$

$$B_{kl}^\dagger\begin{pmatrix} a_k \\ a_l \end{pmatrix} B_{kl} = \begin{pmatrix} \sqrt{T_{kl}} & \sqrt{R_{kl}} \\ -\sqrt{R_{kl}} & \sqrt{T_{kl}} \end{pmatrix}\begin{pmatrix} a_k \\ a_l \end{pmatrix}, \tag{4}$$

and $B_{kl}|00\rangle = |00\rangle$, where $R_{kl} = 1 - T_{kl}$ denotes the reflectance coefficient of the beam splitter. After some algebraic manipulations, it follows from Eq. (2) that

$$M_{ab} = -\sqrt{R_{ac}R_{bc}}|0\rangle_{b,a}\langle 0| + \sqrt{T_{ac}T_{bc}}|1\rangle_{b,a}\langle 1|. \tag{5}$$

Here, we notice that the sign of the first term in Eq. (5) can be changed by simply choosing which beam splitter to deal with. For instance, if we take $B_{ac} = \exp[\theta(ac^\dagger - a^\dagger c)]$, then Eq. (5) becomes $M_{ab} = \sqrt{R_{ac}R_{bc}}|0\rangle_{b,a}\langle 0| + \sqrt{T_{ac}T_{bc}}|1\rangle_{b,a}\langle 1|$. It is clear that the operator M_{ab} in Eq. (5) can be considered as a projection operator, which is composed of a vacuum state and a single-photon state. Thus, any input pure state going through the quantum scissor device is truncated into the superposition of the vacuum state and the single-photon state. For instance, when considering the coherent state as an input $|\alpha\rangle = e^{-|\alpha|^2/2}\sum_{n=0}^{\infty}\alpha^n/\sqrt{n!}|n\rangle$, we have

$$|\psi\rangle_{\rm out} \to |0\rangle_b - g\alpha|1\rangle_b \simeq |g\alpha\rangle_b,\ g = \sqrt{\frac{T_{ac}T_{bc}}{R_{ac}R_{bc}}}. \tag{6}$$

In particular, when $T_{ac} = 1/2$, $T_{bc} = T$, the gain factor is $g_0 = \sqrt{T/(1-T)}$. This result is also obtained in Refs. [26,31]. It is interesting to notice that when these two BSs are asymmetrical, say $T_{ac} = T_{bc} = T$, then $g = T/(1-T) = g_0^2$, i.e., we have a squared gain compared to the original scheme [26,31]. This indicates that using two asymmetrical beam splitters can further enhance the amplification.

For any input mixed state $\rho_{\rm in}$, Eq. (1) becomes

$$\begin{aligned}\rho_{\rm out} &= \frac{1}{p_d} M_{ab}\rho_{\rm in}M_{ab}^\dagger \\ &= \frac{1}{p_d}\Big\{R_{ac}R_{bc}\rho_{\rm in}^{00}|0\rangle_{b,b}\langle 0| + T_{ac}T_{bc}\rho_{\rm in}^{11}|1\rangle_{b,b}\langle 1| \\ &\quad - \sqrt{T_{ac}T_{bc}R_{ac}R_{bc}}\left[\rho_{\rm in}^{01}|0\rangle_{b,b}\langle 1| + \rho_{\rm in}^{10}|1\rangle_{b,b}\langle 0|\right]\Big\},\end{aligned} \tag{7}$$

where, $\rho_{\rm in}^{lm} = \langle l|\rho_{\rm in}|m\rangle$ is the matrix element in Fock space. For thermal state $\rho_{th} = \sum_{n=0}^{\infty}\bar{n}^n/(\bar{n}+1)^{n+1}|n\rangle\langle n|$, the corresponding output state is $\rho_{\rm out} \to [R_{ac}R_{bc}|0\rangle_{b,b}\langle 0| + T_{ac}T_{bc}\bar{n}/(\bar{n}+1)|1\rangle_{b,b}\langle 1|]/(\bar{n}+1)$, in which the nondiagonal elements are absent due to the fact that only diagonal elements are included in the thermal state. It is clear from Eq. (7) that nondiagonal elements ($|0\rangle_{b,b}\langle 1|$ and $|1\rangle_{b,b}\langle 0|$) can be involved in the output state for a general mixed input state. These states can present some interesting nonclassical properties, including but not limited to the squeezing effect and the negative Wigner function. Thus the quantum scissor device plays a role in preparing a highly nonclassical state from a classical state, even for a thermal state.

III. IDEAL QUANTUM SCISSOR DEVICE TO IDEAL TMSVS

In this section, we first consider the ideal quantum scissor device and then move to the ideal TMSVS, i.e., without considering loss effect, detector inefficiency, or an imperfect single-photon source. We start with the single mode and then the two-mode quantum scissor scenario in order to make a comparison between the two.

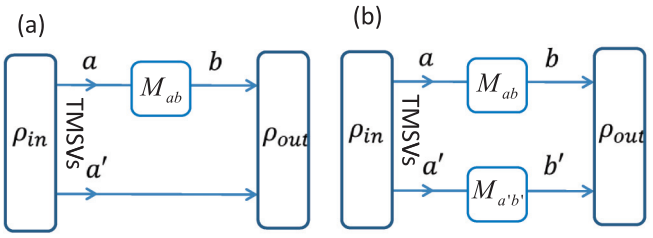

FIG. 2. Scheme of quantum scissors device (QSD) for the TMSV (a) single-side scheme and (b) biside scheme. The relation between input and output can be described by the operator M_{ab} and $M_{a'b'}$.

A. Single-side quantum scissor device to the TMSVS

First we consider one quantum scissor device to one mode of the TMSVS, as shown in Fig. 2(a). Theoretically, the TMSVS is given by

$$|\mathrm{TMSV}\rangle = \mathrm{sech}r \sum_{n=0}^{\infty} \tanh^n r |n, n\rangle_{aa'}, \tag{8}$$

where r is the squeezing parameter and $|n, n\rangle$ are two-mode Fock states. When the single-side quantum scissor device is applied to the TMSVS, it follows from Eqs. (1) and (5) that the output state is

$$|\Psi_S\rangle_{\mathrm{out}} = -(C_{00S}|00\rangle_{b,a'} - C_{11S}|1, 1\rangle_{b,a'}), \tag{9}$$

where $C_{00S} = \sqrt{R_{ac}R_{bc}/p_S}\mathrm{sech}r$, $C_{11S} = \sqrt{T_{ac}T_{bc}/p_S} \times \tanh r \mathrm{sech}r$, and $p_S = (R_{ac}R_{bc} + T_{ac}T_{bc}\tanh^2 r)\mathrm{sech}^2 r$ is the success probability of the single-side quantum scissor device operation. Here the subscript "S" means single side. It is easy to see that the output state is a kind of Bell-like state, which is in two-qubit Hilbert space spanned by the vacuum and the single-photon states, as expected. As a particular case, we choose $C_{00S} = C_{11S}$ leading to $R_{ac}R_{bc} = T_{ac}T_{bc}\tanh^2 r$. Then, Eq. (9) reduces to a Bell state, $\sim(|00\rangle - |1, 1\rangle)/\sqrt{2}$. In addition, if the squeezing parameter r is small, then the TMSVS can be approximated as $(|00\rangle + \tanh r|1, 1\rangle)$, while the output state is $(|00\rangle - g\tanh r|1, 1\rangle)$, where g is defined in Eq. (6). Thus, it is clear that when $g > 1$, one can realize the amplification of the squeezing degree of the TMSVS. A squared gain can also be achieved by two asymmetrical beam splitters compared to the single asymmetrical case.

Next, in order to clearly see the effect of the quantum scissor device on the TMSVS, we further examine the correlation properties by quantifying the degree of entanglement. Here, we use the logarithmic negativity to quantify the degree of entanglement [33], which is an easily computable measure of entanglement. It differs from another measure called entropy of entanglement [34]. The logarithmic negativity is defined by

$$E_\rho = \log_2 \|\rho^{T_A}\|_1, \tag{10}$$

where ρ^{T_A} means the partial transpose of density operator ρ with respect to party A, and the symbol $\|O\|_1$ is the trace norm $\|O\|_1 = \mathrm{tr}|O| = \mathrm{tr}\sqrt{O^\dagger O}$, which is the sum of the singular values of O. For a pure state in the Schmidt form, $|\psi\rangle = \sum_{n=0}^{\infty} c_n|\alpha_n\rangle_a|\beta_n\rangle_b$ with c_n being the normalized factor and $|\alpha_n\rangle_a$ and $|\beta_n\rangle_b$ being orthonormal and normalized states, the logarithmic negativity can be calculated as

$$E_{|\psi\rangle} = \log_2 \left(\sum_{n=0}^{\infty} |c_n|\right)^2. \tag{11}$$

For the TMSVS in Eq. (8), the degree of entanglement is given by $E_{|\mathrm{TMSV}\rangle} = \log_2 e^{2r}$. Similarly, for the pure-state output shown in Eq. (9), the entanglement degree of $|\Psi_S\rangle_{\mathrm{out}}$ can be evaluated as

$$E_{|\Psi_S\rangle_{\mathrm{out}}} = \log_2 \left[1 + \frac{2\sqrt{R_{ac}R_{bc}T_{ac}T_{bc}}\tanh r}{R_{ac}R_{bc} + T_{ac}T_{bc}\tanh^2 r}\right] \leqslant 1. \tag{12}$$

It is interesting to note that the degree of entanglement, $E_{|\Psi_S\rangle_{\mathrm{out}}}$, approaches the maximum value of unity when we choose $R_{ac}R_{bc} = T_{ac}T_{bc}\tanh^2 r$. This corresponds to the Bell-like state. For instance, when $T_{ac} = 1/2$ and $T_{bc} = \cosh^2 r/\cosh 2r$, $|\Psi_S\rangle_{\mathrm{out}} \to (|00\rangle - |1, 1\rangle)/\sqrt{2}$ and $E_{|\Psi_S\rangle_{\mathrm{out}}} = 1$; when $T_{ac} = T_{bc} = T = 1/(1 + \tanh r)$, then $E_{|\Psi_S\rangle_{\mathrm{out}}} = 1$.

In order to clearly see the effect of different parameters T_{ac} and T_{bc} as well as r on the amount of entanglement, we plot the degree of entanglement $E_{|\Psi_S\rangle_{\mathrm{out}}}$ as a function of these three parameters. For a given $T_{ac} = 1/2$, we plot $E_{|\Psi_S\rangle_{\mathrm{out}}}$ and the success probability p_S as a function of T_{bc} and r in Figs. 3(a) and 3(c), respectively. For a comparison, we also show $E_{|\mathrm{TMSV}\rangle}$. It is obvious that the enhanced degree of entanglement can be found in the small squeezing and high-transmission region, say about $0 < r \leqslant 0.35$ and $0.5 \leqslant T_{bc} < 1.0$. In addition, the maximum of $E_{|\Psi_S\rangle_{\mathrm{out}}}$ is equal to unity by modulating the transmissivity according to

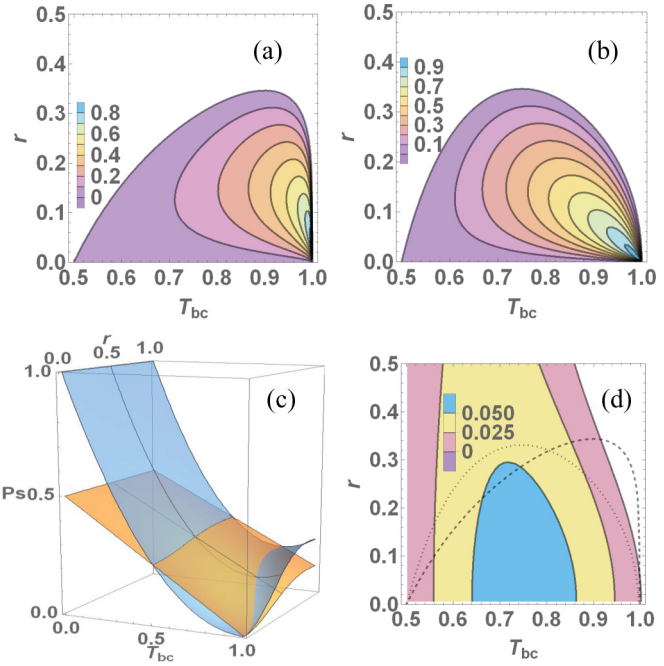

FIG. 3. The logarithmic negativity is plotted as a function of the transmissivity T_{ac} and the squeezing parameter r for given (a) $T_{ac} = 0.5$ and (b) $T_{ac} = T_{bc}$, respectively. The corresponding success probability is shown in (c) and (d). Here, for comparison, the corresponding logarithmic negativity of the TMSV is also plotted (see the dotted line).

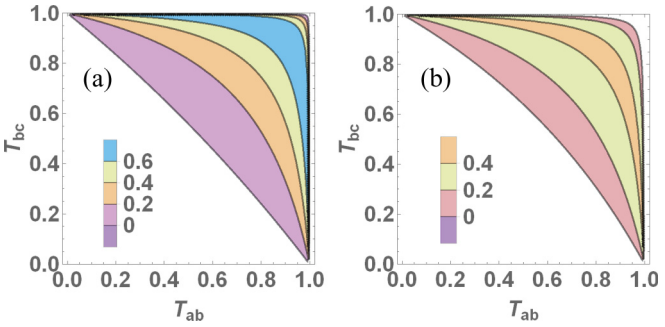

FIG. 4. The difference of logarithmic negativity between the generated state and the TMSVS is plotted as a function of the transmissivity T_{ac} and T_{bc} for the given squeezing parameter (a) $r = 0.1$ and (b) $r = 0.2$, respectively.

$T_{bc} = \cosh^2 r/\cosh 2r$ for a small squeezing parameter r. A similar case is true for the case of $T_{ac} = T_{bc} = T$; see Fig. 3(b). Although the latter can present better performance than the former, the effect is not substantially improved. The difference between these two success probabilities is shown in Fig. 3(d) from which it is clear that the former with $T_{ac} = 1/2$ presents a higher success probability than the latter with $T_{ac} = T_{bc} = T$ in the whole enhanced region. The difference between the two probabilities is small. In Fig. 4, we further analyze the effect of two beam splitters on the entanglement improvement for different values of r. It is clearly shown here that there is a bigger enhanced region, including a low-transmission region for $0 < T_{bc}(T_{ac}) < 0.5$, while it is high for the other region, $0.5 < T_{ac}(T_{bc}) < 1.0$. This implies that for a given small squeezing parameter, one can realize the entanglement improvement in the whole transmission region by introducing two asymmetrical beam splitters. In addition, for a smaller squeezing parameter, the enhance effect is more obvious when a comparison is made between Figs. 4(a) and 4(b). Note that, on one hand, the differences of both performances for entanglement improvement and the success probability are not substantial. On the other hand, in order to realize the same gain factor as the original biside case, we will mainly focus on two asymmetrical beam splitters for the single-side protocol in the following.

B. Biside quantum scissors devices to the TMSVS

In this section, we examine the case when two quantum scissors devices are applied on two modes of the TMSVS, respectively, as shown in Fig. 2(b). In a similar fashion, when deriving Eq. (9) and by using Eq. (5), we have

$$|\Psi_D\rangle_{\text{out}} = C_{00D}|00\rangle_{b,b'} + C_{11D}|1,1\rangle_{b,b'}, \tag{13}$$

where $C_{00D} = \sqrt{R_{ac}R_{bc}R_{a'c'}R_{b'c'}/p_D}\,\text{sech}r$, $C_{11D} = \text{sech}r\tanh r\sqrt{T_{ac}T_{bc}T_{a'c'}T_{b'c'}/p_D}$, and $p_D = (R_{ac}R_{bc}R_{a'c'}R_{b'c'} + T_{ac}T_{bc}T_{a'c'}T_{b'c'}\tanh^2 r)\text{sech}^2 r$ is the success probability. Here, these quantities with prime correspond to the other side quantum scissors device applied on mode a'. It is obvious that when two quantum scissors devices are applied on the TMSVS, the output state has the same form as that of (9), which resulted from the single quantum scissors device except for the negative sign. In fact, the sign difference can be eliminated by modulating the phase of the beam splitter as mentioned above. By comparing p_S and p_D, it is easy to see that the success probability of biside quantum scissors devices is lower than that of the single-side quantum scissors device due to the presence of $T_{a'c'}$ and $T_{b'c'}$. For the original scheme with $T_{ac} = T_{a'c'} = 1/2$, we have $R_{a'c'}R_{b'c'} = T_{a'c'}T_{b'c'} = 1/4$ and the success probability reduces to $p_D = 1/4(R_{bc}R_{b'c'} + T_{bc}T_{b'c'}\tanh^2 r)\text{sech}^2 r$. Thus, when comparing the original scheme with our single-side quantum scissors device scheme (9), it is interesting to see that

$$p_D = \tfrac{1}{4}p_S, \tag{14}$$

when $R_{b'c'} = R_{ac}$. This implies that we can achieve the same entangled state by either a biside quantum scissors device with two symmetrical beam splitters ($T_{ac} = T_{a'c'} = 1/2$) or single-side quantum scissors device with two asymmetrical beam splitters ($T_{ac} = T_{bc} \neq 1/2$). The probability of the latter is four times that of the former. Therefore, the single-side quantum scissors device performs better when considering the enhancement of the entanglement together with the success probability.

Now we turn to the small squeezing parameter r. Both the single-side and the biside quantum scissors devices can achieve enhancement of the degree of squeezing. The gain factors are

$$g_S = \left\{\frac{T_{ac}T_{bc}}{R_{ac}R_{bc}}\right\}^{1/2}, \quad g_D = \left\{\frac{T_{ac}T_{bc}T_{a'c'}T_{b'c'}}{R_{ac}R_{bc}R_{a'c'}R_{b'c'}}\right\}^{1/2}, \tag{15}$$

for the single-side and biside quantum scissors devices, respectively. For asymmetrical beam splitters and taking $T_{ac} = T_{bc} = T_{a'c'} = T_{b'c'}$, we obtain

$$g_D = g_S^2 = g_0^4. \tag{16}$$

Compared to Ferreyrol *et al.*'s scheme with $g_0 = \sqrt{T}/\sqrt{1-T}$, from Eq. (16) it is clear that a squared and a biquadrate gain can be obtained, respectively, by single-side and biside quantum scissors operations. The reason for $g_S = g_0^2$ is due to the presence of two asymmetrical beam splitters in the single side of the quantum scissors device, in which the asymmetry is a necessary condition for the amplification, while the reason for $g_D = g_S^2$ lies in the fact that a biside quantum scissors device amplifies the single-photon coefficient weight twice. In particular, the single-side quantum scissors device with two asymmetrical beam splitters can achieve the same entangled state with a higher success probability as the biside original quantum scissors device. Thus, in order to realize a higher squeezing amplification for the TMSVS, it is better to use two asymmetrical beam splitters in a set of quantum scissors device.

IV. IDEAL QUANTUM SCISSORS DEVICE TO THE REALISTIC TMSVS

In a realistic scenario, a quantum system undergoes decoherence as a result of interaction with its environment. This motivates us to go beyond the ideal TMSVS to a realistic scenario, i.e., passing through a dissipative channel (see Fig. 5). For simplicity, we examine two symmetrical photon

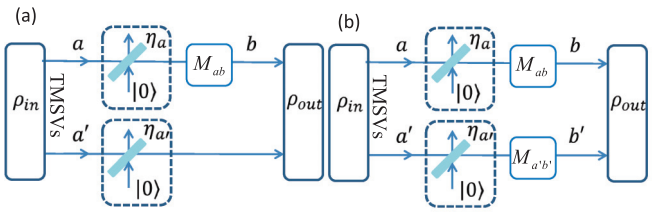

FIG. 5. Scheme of the QSD for the realistic TMSV (a) single-side case and (b) biside case. The relation between output and input can be described by operator M_{ab} and $M_{a'b'}$.

loss channels with transmission coefficient η_t. In view of the transformation property of the quantum scissors device as shown in Eq. (5), it is convenient to discuss photon loss in Fock space. For this purpose, we derive the normal ordering form of the output state.

A. Output state after channel loss

In order to obtain the output state after channel loss, it is often convenient to use the Wigner function in phase space. Using the formula connecting the Wigner function of the output and the initial states for the single-mode case [35],

$$W_{\rm out}(q_1,p_1)=\int\frac{dq'dp'}{\pi\eta_r}W_{\rm in}(q_1',p_1')\times e^{-\frac{1}{\eta_r}[(q_1-\sqrt{\eta_t}q_1')^2+(p_1-\sqrt{\eta_t}p_1')^2]},\tag{17}$$

where $W_{\rm in}(q_1',p_1')$ is the initial Wigner function of the single-mode system, whose definition in the coordinate state representation is given by

$$W(q_1',p_1')=\int\frac{dy}{2\pi}e^{iyp_1'}\left\langle q_1'-\frac{y}{2}\middle|\rho\middle|q_1'+\frac{y}{2}\right\rangle=\mathrm{Tr}[\rho\Delta_1(q_1',p_1')].\tag{18}$$

Here, $\Delta_1(q_1,p_1)$ is the Wigner operator,

$$\Delta_1(q_1',p_1')=\int\frac{dye^{iyp_1'}}{2\pi}\left|q_1'+\frac{y}{2}\right\rangle\left\langle q_1'-\frac{y}{2}\right|.\tag{19}$$

When each mode of the TMSVS independently goes through a loss channel, the output Wigner function can be calculated as

$$W_{\rm out}(q_1,p_1,q_2,p_2)=\int\frac{dq_1'dp_1'dq_2'dp_2'}{(\pi\eta_r)^2}W_{\rm in}(q_1',p_1',q_2',p_2')\times e^{-\frac{1}{\eta_r}[(q_1-\sqrt{\eta_t}q_1')^2+(p_1-\sqrt{\eta_t}p_1')^2]}\times e^{-\frac{1}{\eta_r}[(q_2-\sqrt{\eta_t}q_2')^2+(p_2-\sqrt{\eta_t}p_2')^2]},\tag{20}$$

where $W_{\rm in}(q_1',p_1',q_2',p_2')=\mathrm{Tr}[\rho\Delta_1(q_1',p_1')\Delta_2(q_2',p_2')]$. Thus the Wigner function after the TMSVS through photon loss is given by

$$W_{\rm out}(q_1,p_1,q_2,p_2)=\frac{B_1}{\pi^2}\exp\{2B_3(q_1q_2-p_1p_2)\}\times\exp\{-B_2(p_1^2+p_2^2+q_1^2+q_2^2)\},\tag{21}$$

where we define $\eta_r=1-\eta_t$, and

$$B_1=\frac{1}{1+4\eta_t\eta_r\sinh^2 r},\tag{22}$$

$$B_2=\frac{\eta_r+\eta_t\cosh 2r}{1+4\eta_r\eta_t\sinh^2 r},\tag{23}$$

$$B_3=\frac{\eta_t\sinh 2r}{1+4\eta_r\eta_t\sinh^2 r}.\tag{24}$$

It is interesting to note that the Wigner function of the output is similar to the initial Wigner function, which indicates that the Gaussian nature of the TMSVS can be kept after photon loss [3,36]. In particular, when $\eta_t=0$ corresponds to the case without photon loss, Eq. (21) just reduces to the initial Wigner function. From the Wigner function, we can derive the density operator by using the formula

$$\rho=(2\pi)^2\int W(\vec{q})\Delta(\vec{q})dq_1dp_1dq_2dp_2,\tag{25}$$

where $\vec{q}=(q_1,p_1,q_2,p_2)$, $\Delta(\vec{q})=\Delta(q_1,p_1)\otimes\Delta(q_2,p_2)$ and $\Delta(q,p)$ is called the Wigner operator, whose normal ordering form is given by [37]

$$\Delta(q,p)=\frac{1}{\pi}:\exp\{-(q-Q)^2-(p-P)^2\}:,\tag{26}$$

with $Q=(a+a^\dagger)/\sqrt{2}$, $P=(a-a^\dagger)/(i\sqrt{2})$. Here, the symbol $:\cdots:$ represents the normal ordering. On substituting Eqs. (21) and (26) into Eq. (25), we obtain

$$\rho_{\rm bef}=C_1:e^{-C_2(a^\dagger a+a'^\dagger a')+C_3(a^\dagger a'^\dagger+aa')}:,\tag{27}$$

where $\rho_{\rm bef}$ is the density operator before the quantum scissors device, and

$$C_1=\frac{\mathrm{sech}^2 r}{1-\eta_r^2\tanh^2 r},\tag{28}$$

$$C_2=\frac{1-\eta_r\tanh^2 r}{1-\eta_r^2\tanh^2 r},\tag{29}$$

$$C_3=\frac{\eta_t\tanh r}{1-\eta_r^2\tanh^2 r}.\tag{30}$$

We expect that $\rho_{\rm bef}$ in Eq. (27) is still of a Gaussian form. Using the coherent-state representation of the Fock state, i.e., $|m\rangle=1/\sqrt{m!}\frac{\partial^m}{\partial t^m}\|t\rangle|_{t=0}$ where $\|t\rangle=e^{ta^\dagger}|0\rangle$ is the unnormalized coherent state, the matrix elements of $\rho_{\rm bef}$ in Fock space can be obtained as

$$\rho_{\rm bef}=\sum_{m,n,m',n'=0}^{\infty}C_{m,n,m',n'}|m,n\rangle\langle m',n'|,\tag{31}$$

where we use $\langle v\|t\rangle=e^{vt}$ and define

$$C_{m,n,m',n'}=\widehat{D}\left.\frac{e^{-(C_2-1)(\mu\tau+\nu t)+C_3(\mu\nu+\tau t)}}{\sqrt{m!n!m'!n'!}/C_1}\right|_{\tau,t,\mu,\nu=0},\tag{32}$$

as well as $\widehat{D}\equiv\partial^{m+n+m'+n'}/\partial\mu^m\partial\nu^n\partial\tau^{m'}\partial t^{n'}$.

B. Ideal quantum scissor devices to the realistic TMSVS

We start by considering the single quantum scissor device applied to the realistic TMSVS, i.e., operating a single-side quantum scissor device to one mode of the realistic TMSVS

[see Fig. 5(a)]. From Eq. (7), it is clear that we need to calculate $\rho_{\rm bef}^{00}$, $\rho_{\rm bef}^{01}$, $\rho_{\rm bef}^{10}$, and $\rho_{\rm bef}^{11}$. Using Eq. (27) or Eq. (31), we obtain

$$\rho_{\rm bef}^{00} = \frac{C_1}{C_2}\rho_{th,a'}(\bar{x}), \tag{33}$$

$$\rho_{\rm bef}^{01} = \frac{C_1 C_3}{C_2}\rho_{th,a'}(\bar{x})a', \tag{34}$$

$$\rho_{\rm bef}^{10} = \frac{C_1 C_3}{C_2}a'^{\dagger}\rho_{th,a'}(\bar{x}), \tag{35}$$

$$\rho_{\rm bef}^{11} = \frac{C_1 C_3^2}{C_2}a'^{\dagger}\rho_{th,a'}(\bar{x})a' + \bar{x}C_1\rho_{th,a'}(\bar{x}), \tag{36}$$

where $\rho_{th,a'}(\bar{x})$ is the thermal state with average number $\bar{x} = (1-C_2)/C_2$. On substituting Eqs. (33)–(36) into Eq. (7), the resulting expression of $\rho_{\rm out}^S$ is

$$\begin{aligned}\rho_{\rm out}^S = \frac{C_1}{\bar{p}_S}\Bigg\{ & T_{ac}T_{bc}\frac{C_3^2}{C_2}a'^{\dagger}\rho_{th,a'}(\bar{x})a'|1\rangle_{b,b}\langle 1| \\ & + \rho_{th,a'}(\bar{x})\left(\frac{R_{ac}R_{bc}}{C_2}|0\rangle_{b,b}\langle 0| + T_{ac}T_{bc}\bar{x}|1\rangle_{b,b}\langle 1|\right) \\ & - \mathfrak{T}[\rho_{th,a'}(\bar{x})a'|0\rangle_{b,b}\langle 1| + a'^{\dagger}\rho_{th,a'}(\bar{x})|1\rangle_{b,b}\langle 0|]\Bigg\},\end{aligned} \tag{37}$$

where we can see that the third term has certain coherence and $\mathfrak{T} = \{T_{ac}T_{bc}R_{ac}R_{bc}\}^{1/2}C_3/C_2$.

In order to clearly see the property of $\rho_{\rm out}^S$, we consider the space spanned by Fock state $(|0\rangle, |1\rangle)$, which is a good approximation for a weak squeezing parameter r. Here, for simplicity, we take $T_{ac} = T_{bc} = T$, $R_{ac} = R_{bc} = R$ for the single-side quantum scissor device case. Under Fock representation of the thermal state,

$$\rho_{th}(u) = \sum_{m=0}^{\infty}\frac{u^m}{(u+1)^{m+1}}|m\rangle\langle m|, \tag{38}$$

Eq. (37) can be rewritten as

$$\begin{aligned}\rho_{\rm out}^S = \frac{\operatorname{sech}^2 r}{\bar{p}_S}\Big\{ & R^2|\psi_{\rm out}^S\rangle\langle\psi_{\rm out}^S| + \tanh^2 r\big[\eta_r^2 R^2|00\rangle_{ba',ba'}\langle 00| \\ & + \eta_t\eta_r T^2|10\rangle_{ba',ba'}\langle 10| + \eta_t\eta_r R^2|01\rangle_{ba',ba'}\langle 01|\big]\Big\},\end{aligned} \tag{39}$$

where we have dropped high-order terms, which are less than $\eta_r^2\tanh^2 r$, and set

$$|\psi_{\rm out}^S\rangle = |00\rangle_{ba'} - \frac{T}{R}\eta_t\tanh r|11\rangle_{ba'}. \tag{40}$$

Thus, there is a coherence in the first term of $\rho_{\rm out}^S$.

Next, we consider the case of biside quantum scissors devices applied to the realistic TMSVS [see Fig. 5(b)]. In a similar fashion to the derivation of Eqs. (37), (39), and (40), and according to Eqs. (7) and (37), we obtain

$$\begin{aligned}\rho_{\rm out}^D = \frac{\operatorname{sech}^2 r}{4\bar{p}_D}\Big\{ & R^2|\psi_{\rm out}^D\rangle\langle\psi_{\rm out}^D| + \tanh^2 r\big[\eta_r^2 R^2|00\rangle_{bb',bb'}\langle 00| \\ & + \eta_t\eta_r TR|10\rangle_{bb',bb'}\langle 10| + \eta_t\eta_r TR|01\rangle_{bb',bb'}\langle 01|\big]\Big\},\end{aligned} \tag{41}$$

where, for simplicity, we have taken $T_{ac} = T_{a'c'} = 1/2$ and $T_{bc} = T_{b'c'} = T$, as well as $R_{bc} = R_{b'c'} = R$, and

$$|\psi_{\rm out}^D\rangle = |00\rangle + \frac{T}{R}\eta_t\tanh r|11\rangle. \tag{42}$$

One can see that $|\psi_{\rm out}^D\rangle$ and $|\psi_{\rm out}^S\rangle$ can have the same form. In addition, $\rho_{\rm out}^D$ can be described fully in 0-1 photon subspace, which is different from $\rho_{\rm out}^S$. This point is clear by looking at Eq. (7).

For a small squeezing TMSVS, $|\text{TMSV}\rangle$ can be approximately rewritten as $|\text{TMSV}\rangle \to |00\rangle + \tanh r|11\rangle$. From Eq. (40), one can realize the amplification of the TMSVS by choosing T such that $T > 1/(1+\eta_t)$ even in the present of photon loss. Furthermore, it is obvious that a squared gain improvement can still be achieved compared to that of Ferreyrol *et al.*'s scheme [31], in which $g_0 = \sqrt{T}/\sqrt{1-T}$. This amplification implies that the degree of entanglement can still be improved by the single-side and biside quantum scissors operation even after the TMSVS goes through a dissipative channel.

1. Total entanglement

We again examine the entanglement using logarithmic negativity defined in Eq. (10) but with an inclusion of the photon losses. Using Eqs. (39) and (41), we have

$$E_{\rho_{\rm out}^{S,D}} = \log_2\left(\sum_{i=1}^{4}|\lambda_i|\right), \tag{43}$$

where λ_i are the eigenvalues of partial transpose density operator $(\rho_{\rm out}^{S,D})^{T_b}$ (see Appendices A and B for more details).

In Fig. 6, we plot the entanglement as a function of squeezing parameter for some given values of T and η_t. For comparison, we also plot the entanglement degrees of the ideal and dissipated TMSVS. Both cases are also plotted when the quantum scissors device is absent. It is clear that for $\eta_t = 1$, the same enhanced level is shared by both single-side and biside quantum scissors devices. As r increases, the enhanced degree initially increases within a small squeezing region and then decreases. The maximal squeezing parameter r, which corresponds to the enhanced region, becomes smaller, while the maximal degree of entanglement becomes bigger as T increases. When considering the effect of photon loss, there is a somewhat different performance in these two cases. For a given dissipation of, say, $\eta_t = 0.9$, although the biside quantum scissors devices presents a better performance than the single-side quantum scissors device, this advantage becomes less obvious as the transmissivity T decreases [see Fig. 6(a)]. For a given $T = 0.92$, the effects of different dissipation are presented in Fig. 6(b). It is clear that under given $\eta_t = 0.90, 0.85$, the entanglement is almost kept unchanged for the biside quantum scissors device case, while for the single-side case, there is a certain reduction, which becomes more obvious as squeezing parameter r increases. This indicates that the biside quantum scissors device case is more robust against the environment than the single-side quantum scissors device case.

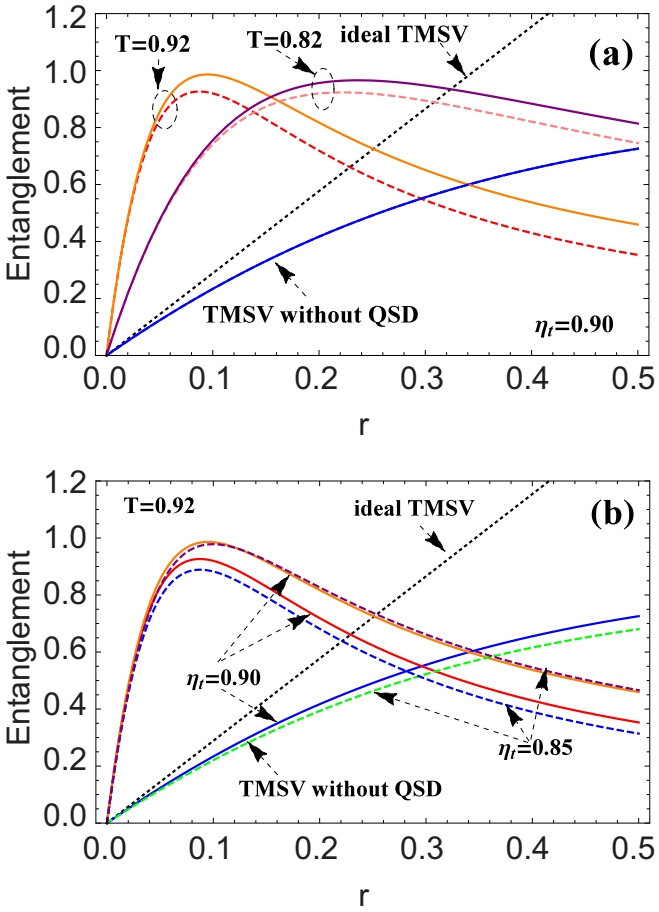

FIG. 6. The logarithmic negativity is plotted as a function of squeezing parameter r for given transmissivity T and dissipative η_t: (a) $\eta_t = 0.90$ and $T = 0.92, 0.82$, and (b) $T = 0.92$, $\eta_t = 0.9, 0.85$, respectively. The corresponding logarithmic negativity of the TMSV is also plotted (see black dotted line).

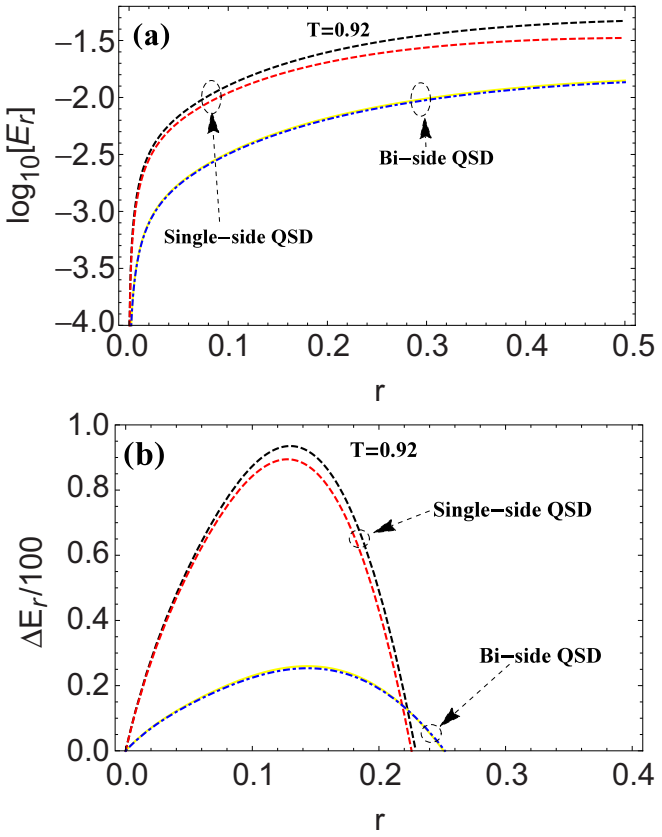

FIG. 7. The logarithmic negativity is plotted as a function of squeezing parameter r for given transmissivity $T = 0.92$ and dissipative $\eta_t = 0.90, 0.88$ for (a) the entanglement rate E_r and (b) the enhancement rate of entanglement ΔE_r, respectively.

2. Entanglement enhanced rate

Success probability is an important factor for the nondeterministic operation. The success probabilities for the generated output states for both single-side and biside quantum scissors devices cases using Eqs. (39) and (41), respectively, are given by

$$\bar{p}_S = \mathrm{sech}^2 r[R^2 + (R^2 + \eta_t - 2R\eta_t)\tanh^2 r], \tag{44}$$

$$\bar{p}_D = \frac{\mathrm{sech}^2 r}{4}[R^2 + (R + \eta_t - 2R\eta_t)^2 \tanh^2 r]. \tag{45}$$

The success probabilities depend on R, r, and dissipation factor η_t. One particular case is when $\eta_t = 1$ corresponding to the lossless case. In that case, Eqs. (44) and (45) reduce to those of the ideal cases above, as expected. Comparing p_S with p_D, it is clear that

$$\bar{p}_S \geqslant 4\bar{p}_D, \tag{46}$$

where the equal sign holds for $\eta_t = 0, 1$ or $R = 1/2$. Thus, the success probability of the single-side quantum scissors device is four times more than that of the biside quantum scissors devices when the photon-loss case is considered.

In order to consider the effect of both entanglement and success probability, we can use the product of entanglement and probability together, i.e., the entanglement rate [21] $E_r = E(\rho)p(\rho)$, which gives the average entanglement per trial of the scheme. From Fig. 7(a), it is clear that the entanglement rate of the single side is higher than that of the biside. In Fig. 7(b), we show the enhancement rate of entanglement, which is defined as the average increase per trial, i.e., $\Delta E_r = p(\rho)[E(\rho) - E(\rho_{\mathrm{init}})]$, where ρ and ρ_{init} are the final and initial states, respectively. Again, for given $T = 0.92$, $\eta_t = 0.90, 0.88$, Fig. 7(b) shows that the single-side quantum scissors device performs better than the biside quantum scissors devices within the range $0 < r < 0.23$, and the opposite is true within $0.23 < r < 0.25$. These results indicate that the single-side quantum scissors device presents a better performance than the biside quantum scissors device in a wider squeezing range.

V. REALISTIC QUANTUM SCISSORS DEVICE TO THE REALISTIC TMSVS

So far we looked at the scenario where an ideal single-photon state and an ideal single-photon detector are used. However, this is not the case when we consider a realistic situation. On one hand, it is inevitable that the photon state can interact with the environment. On the other hand, both

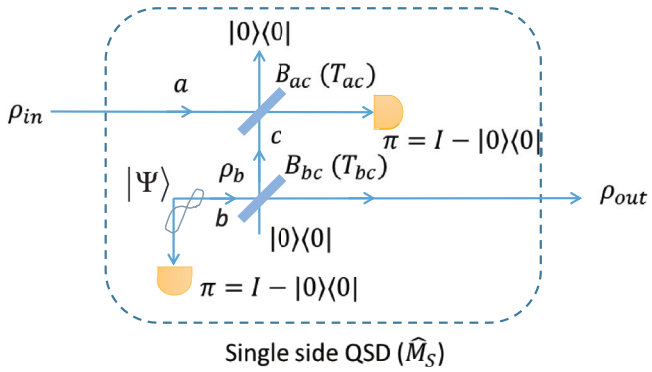

FIG. 8. Realistic scheme of a single-side QSD for any input state $\rho_{\rm in}$. The beam splitters ($\rm BS_{ac}$ and $\rm BS_{bc}$) are asymmetrical with transmission coefficients T_{ac} and T_{bc}, respectively. The relation between output and input can be described by operator $\hat{M}_S$. And the heralded single photon is generated from the two-mode squeezed state $|\Psi\rangle$. Here, all detectors are dichotic "on-off" detectors.

the perfect single-photon source and single-photon detector are difficult to obtain experimentally. Hence, in order to consider a more realistic scenario, we replace the single-photon level detector with the "on-off" detector $\Pi = 1 - |0\rangle\langle 0|$ and use a conditional measurement with the parametric down-conversion state $|\Psi\rangle = \mathrm{sech}\lambda \sum_{m=0}^{\infty} \tanh^m \lambda |m, m\rangle$ (8) to generate the single-photon state [29]. To avoid confusion, we should mention that λ here is the squeezing parameter of the TMSV used for the b port in Fig. 8 which is fixed and r is the squeezing parameter of the input state $\rho_{\rm in}$ which is a varying variable. Here, the conditional measurement is also realized by the on-off detector (see Fig. 8). In this case, we use the on/off-type detector where we can only distinguish whether or not there is a photon. We do not distinguish the photon number, so there can be a photon number larger than 1. In the following numerical calculation, we truncated the photon number to 5, which is a very good approximation when the average photon is small. Thus, the heralded single-photon state (HSPS) ρ_b (normalized state) after detection by Π is given by

$$\rho_b = \frac{1}{\bar{n}}[(\bar{n}+1)\rho_{th}(\bar{n}) - |0\rangle_{bb}\langle 0|], \tag{47}$$

where $\rho_{th}(\bar{n}) = \sum_{m=0}^{\infty} \bar{n}^m/(\bar{n}+1)^{m+1}|m\rangle\langle m|$ is the thermal state with $\bar{n} = \sinh^2\lambda$ being the average photon number. It is a good approximation to talk about the single-photon state when the squeezing parameter λ is very small. The HSPS ρ_b can be seen as a superposition of the thermal state and vacuum. This property shall be used in the following calculation.

A. Relation between input and output states

In order to deal with the realistic quantum scissors device, we first consider a single-mode input state (shown in Fig. 8). Moreover, for any single-mode density operator ρ_a, after the single quantum scissors device, the output state $\rho_{\rm out}$ can be expressed as

$$\rho_{\rm out} = N\mathrm{Tr}_{ac}[\Pi_a|0\rangle_{cc}\langle 0|B_{ac}B_{bc}\rho_a\rho_b|0\rangle_{cc}\langle 0|B_{bc}^{\dagger}B_{ac}^{\dagger}], \tag{48}$$

where N is the normalization factor determined by $\mathrm{Tr}_b\rho_{\rm out} = 1$. Similar to the above discussion of Eq. (1), the output state $\rho_{\rm out}$ can also be put into the following form (see Appendix C for details):

$$\rho_{\rm out} = N\mathrm{Tr}_a[(\Lambda_{ab} - \Lambda_b|0\rangle_{aa}\langle 0|)\rho_a], \tag{49}$$

where we have set

$$\Lambda_{ab} = \frac{1}{\bar{n}}[\Omega(\bar{n}+1) - (T_{ac})^{a^{\dagger}a}|0\rangle_{bb}\langle 0|], \tag{50}$$

$$\Lambda_b = \frac{1}{\bar{n}}\left[\frac{x(\bar{n}+1)}{\bar{n}T_{bc}}\rho_{th}(x) - |0\rangle_{bb}\langle 0|\right], \tag{51}$$

in which $\rho_{th}(x)$ is the thermal state with average photon number $x = \bar{n}T_{bc}/(\bar{n}R_{bc}+1)$, and

$$\Omega = A_1 : e^{-[A_2a^{\dagger}a + A_3b^{\dagger}b + A_4(a^{\dagger}b + b^{\dagger}a)]} : . \tag{52}$$

Here, $A_j (j = 1, 2, 3, 4)$ are defined in Eqs. (C22)– (C25) in Appendix C.

When the single-side quantum scissors device is applied to one mode of any two-mode system (denoted as $\rho_{aa'}$), the yielded output state is $\rho_{\rm out}^S$ from Eq. (49), i.e.,

$$\rho_{\rm out}^S = N\mathrm{Tr}_a[(\Lambda_{ab} - \Lambda_b|0\rangle_{aa}\langle 0|)\rho_{aa'}], \tag{53}$$

while for both modes independently going through quantum scissors devices, the output state $\rho_{\rm out}^D$ is

$$\rho_{\rm out}^D = N\mathrm{Tr}_{aa'}\{\rho_{aa'}(\Lambda_{ab} - \Lambda_b|0\rangle_{aa}\langle 0|)| \otimes(\Lambda_{a'b'} - \Lambda_{b'}|0\rangle_{a'a'}\langle 0|)\}. \tag{54}$$

Based on Eq. (53) or (54), one can derive the normal ordering form of the output state when the input state $\rho_{aa'}$ is known. Here, for convenience, we only consider the single-side quantum scissors device due to its advantage in both success probability and enhanced entanglement, which are analyzed in Sec. III.

Substituting Eq. (27) into Eq. (53), one can finally obtain the output density operator (see Appendix D),

$$\rho_{\rm out}^S = N\{\widehat{O} - P_2\rho_{th,a'}(y)\rho_{th}(x) + [P_3\rho_{th,a'}(y) - P_1\rho_{th,a'}(z)]|0\rangle_{bb}\langle 0|\}, \tag{55}$$

where $N^{-1} = \mathrm{Tr}(\widehat{O}) - P_1 - P_2 + P_3$, $\widehat{O}$ (normal ordering form) and y, z, and $P_j (j = 1, 2, 3)$ are defined in Appendix D (not shown here for convenience). $\rho_{th,a'}(u)$ is a thermal state for mode a' with average photon number u. From Eq. (55), it is clear that the output state is composed of two-mode entangled state $\widehat{O}$, thermal, and vacuum states. With the help of Eq. (55), one can evaluate the output state in the form of density matrix and phase space.

B. Entanglement enhancement

Except for $\widehat{O}$, the other three terms only have the diagonal elements as shown in Eq. (55). In order to calculate the degree of entanglement using Eq. (10), in a similar fashion to Eq. (32), one needs to expand $\widehat{O}$ in Fock space to get the factor

$$O_{mnm'n'} = \widehat{D}\frac{e^{(1-W_2)\mu\tau + (1-W_3)\nu t - W_4(\mu\nu+\tau t)}}{\bar{n}\sqrt{m!n!m'!n'!}/[(\bar{n}+1)W_1]}\Bigg|_{\mu,\nu,\tau,t=0}. \tag{56}$$

And, hence, using Eqs. (55) and (56), we can numerically evaluate the degree of entanglement. Here it should be emphasized that Eq. (56) is obtained when the single-side quantum scissors device is applied to one mode of the dissipated

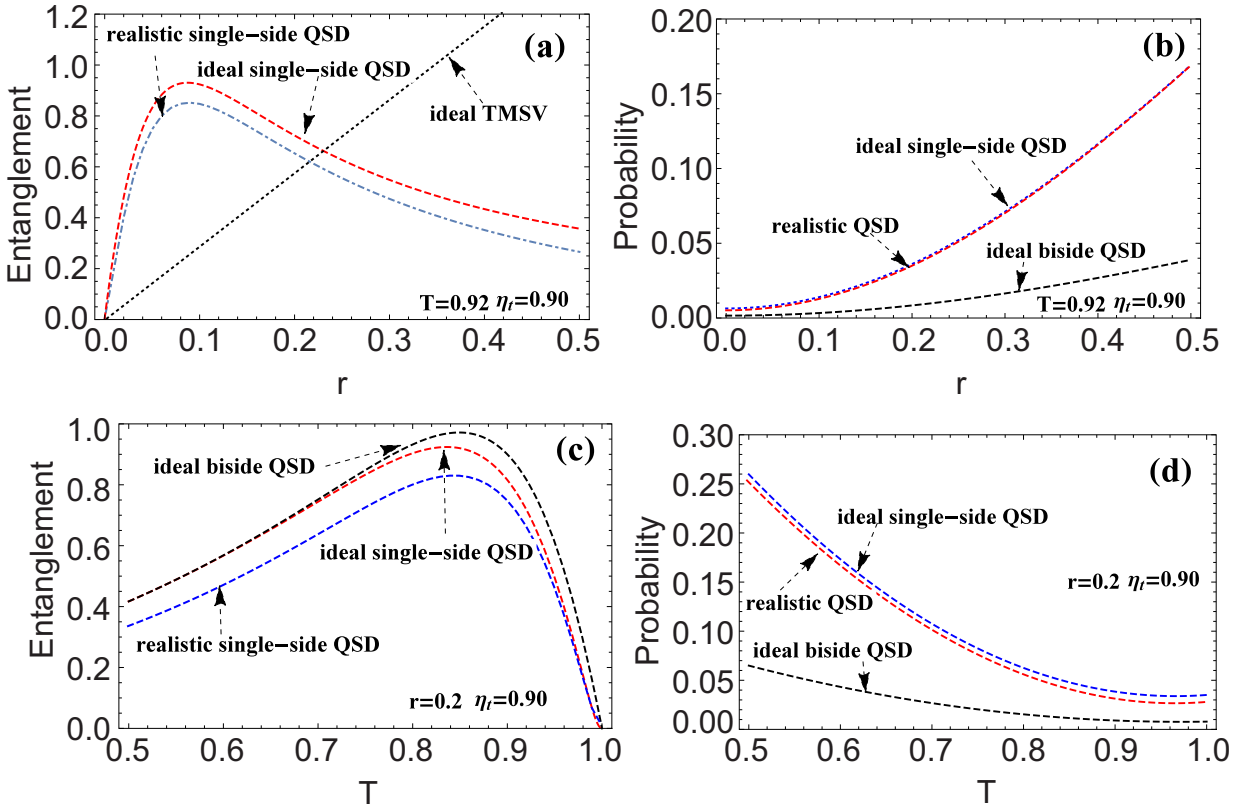

FIG. 9. The entanglement degree and success probability as a function of squeezing parameter r and transmission efficiency T, for $\eta_t = 0.9$, $\lambda = 0.2$, and (a),(b) $T = 0.92$, and (c),(d) $r = 0.2$.

TMSVS, where the TMSVS is assumed to be transmitted through the biside symmetrical photon-loss channel with the same efficiency η_t.

In Fig. 9, we plot the entanglement degree and the success probability N^{-1} as a function of squeezing parameter and transmission efficiency, for some given parameters. From Fig. 9(a), there is clear evidence that (i) entanglement improvement still takes place in a small squeezing region ($0 \leqslant r \leqslant 0.22$), even when the realistic quantum scissors device is applied to a realistic TMSVS; (ii) in this realistic situation, both the maximum of enhanced entanglement (about 0.854) and the region of r, which corresponds to the same enhanced entanglement region, are slightly smaller than the case when the ideal quantum scissors device is applied to a realistic TMSVS, where the maximum and the region are about 0.934 and $0 \leqslant r \leqslant 0.23$. However, one should notice that they almost share the same success probability [see Fig. 9(b)]. For given $r = 0.2$ and $\eta_t = 0.9$, Fig. 9(c) shows that the entanglement initially increases and then decreases as T increases, while Fig. 9(d) shows different behavior, where the success probability decreases with the increase of T. Our results show that there is no clear-cut difference between the ideal quantum scissors device and realistic quantum scissors device, of course, within the situations that we consider.

C. Comparison with quantum catalysis

Next we make a comparison with another entanglement distillation scheme, namely, the quantum catalysis. The quantum catalysis, here, is on the TMSVS and we assume that both modes go through beam splitters with equal transmission T_C. One can refer to Refs. [11,13,18,21,38,39] for other non-Gaussian distillation schemes. Notice that for our current scheme, the entanglement can be improved within the high-transmission and low squeezing region using the quantum scissors device [see Fig. 10(a)]. It seems that the region of T, which corresponds to the enhanced entanglement, becomes smaller as r increases. However, for the quantum catalysis case in Ref. [20], it is shown there that the entanglement of the TMSVS can also be enhanced by quantum catalysis, but within a low region of transmission T_C ($0 < T_C < 0.26$) and a small squeezing region ($0 < r < 0.57$); see Fig. 10(b). Looking at Figs. 10(a) and 10(b), one can see that the maximal value of enhanced entanglement by quantum catalysis is slightly larger than unity, while unity is just the upper bound that is obtained by the quantum scissors device. The reason may be that the optimal output after the quantum scissors device is very similar to that of the Bell-like state $[(|00\rangle + |11\rangle)/\sqrt{2}]$, especially in an ideal case.

Quantum catalysis and quantum scissors schemes have different success probabilities for different transmission and squeezing parameters, which makes comparison somewhat difficult. Thus, we only consider the enhanced scenario to compare the success probabilities. In Figs. 10(c) and 10(d), we plot the success probabilities as a function of parameter r and transmissivity $T(T_C)$ for some given parameters. From Fig. 10(c), and for given $T_C = 0.1$ and $T = 0.8$, it is interesting to see that both single-side operations (for catalysis

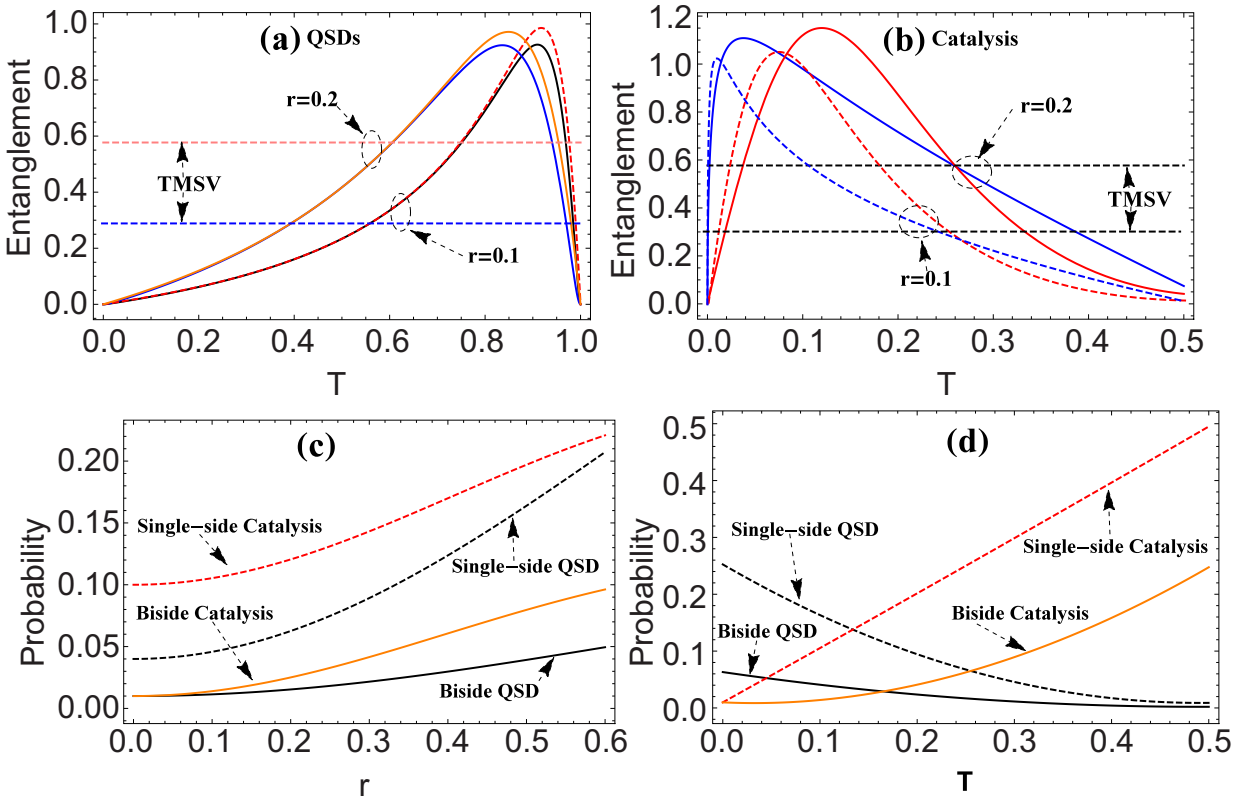

FIG. 10. The entanglement of the output state (a) after QSD and (b) after catalysis, as a function of transmission for several given squeezing parameters $r = 0.1, 0.2$ and $\eta_t = 0.9$. Single-side QSD: black and blue; two-side QSD: red and orange. For comparison, the entanglement of the TMSVS is also plotted in dashed blue and dashed pink for $r = 0.1, 0.2$, respectively. (c) Success probability as a function of (c) r for given T, and (d) T for given r with $\eta_t = 0.9$.

and quantum scissors) present a higher success probability than those of biside operations. The single-side catalysis has the largest success probability, while the second one is the single-side quantum scissors device. But when we have the squeezing parameter $r = 0.1$, one can find that there is a higher success probability for the quantum scissors device, not the quantum catalysis, in a certain transmission region [see Fig. 10(d)]. Thus, in order to generate the expected output states effectively, one needs to seek the optimal trade-off between the success probability and the figure of merits by adjusting the squeezing parameter r and the transmission rate.

VI. CONCLUSION

In this work, we proposed a modified quantum scissor scheme to improve both quantum state amplification and entanglement. Squared gain can be secured using our scheme compared to the original amplification scheme for a single-mode quantum state. Along with the effects of the modified quantum scissor scheme, we considered the original scheme of the TMSVS entanglement. Our scheme helps to obtain the same squared gain for a squeezing parameter when applied to the single side of the TMSVS as opposed to applying the original scheme to the biside of the TMSVS. In this case, our scheme uses not only less resources and less energy, but also helps to enhance entanglement by a factor of four with the success probability of the biside scheme. We investigated the effect of the environment on the entanglement and the success probability. We found that even when both modes of the TMSVS go through a photon-loss channel, a realistic single-side quantum scissors device can still play a role in enhancing the entanglement if the initial squeezing is small. The entanglement enhancement effect in this case is slightly smaller than that of the ideal single-side quantum scissors device. The success probability is almost the same as that of the ideal single-side quantum scissors device. These results reveal the usefulness of the single-side quantum scissors device characteristic of two asymmetrical beam splitters for improving the gain and the entanglement as well as the ability to work in the present of the decoherence. This also provides a useful insight for applying such scheme for long-distance quantum communication. In addition, we also provide a concise way to calculate the output state using the operator form.

Non-Gaussian operations have been applied to many fields, such as quantum key distribution and quantum steering with continuous variables to improve their performance [40–43]. In quantum key distribution, the success probability is an important factor describing the secret key rate, and the single-side non-Gaussian operation, not the biside, is a more practical protocol. Furthermore, asymmetry is an important characteristic of quantum steering, which has become a kind of key source for single-side device-independent quantum information protocols. Thus, our current investigation should be beneficial for further consideration when

such quantum scissors device non-Gaussian operation is applied to quantum key distribution and quantum steering. It should help to improve the transmission distance and either one-way or two-way steering. These features will be examined later.

ACKNOWLEDGMENTS

This work is supported by a grant from the King Abdulaziz City for Science and Technology (KACST). L.H. is supported by the National Natural Science Foundation of China (Grants No.11664017 and No. 11964013), as well as the Outstanding Young Talent Program of Jiangxi Province (Grant No. 20171BCB23034). Z.L. is supported by a startup Grant (No. 74130-18841222) at Sun Yat-sen University.

APPENDIX A: ENTANGLEMENT FOR DENSITY OPERATOR SHOWN IN EQ. (39)

First we rewrite Eq. (39) as

$$\rho_{\rm out}^{S} = c_1|00\rangle\langle 00| + c_2|11\rangle\langle 11| + c_3|10\rangle\langle 10| + c_4|01\rangle\langle 01| - c_5(|00\rangle\langle 11| + |11\rangle\langle 00|)], \tag{A1}$$

or

$$\rho_{\rm out}^{S} = \begin{pmatrix} c_1 & 0 & 0 & -c_5 \\ 0 & c_4 & 0 & 0 \\ 0 & 0 & c_3 & 0 \\ -c_5 & 0 & 0 & c_2 \end{pmatrix}, \tag{A2}$$

where $\rho_{\rm out}^{S}$ is a real and symmetrical matrix, and c_j are defined by

$$c_1 = \frac{\operatorname{sech}^2 r}{p_S} R^2\left(1 + \eta_r^2 \tanh^2 r\right), \tag{A3}$$

$$c_2 = \frac{\operatorname{sech}^2 r}{p_S} T^2 \eta_t^2 \tanh^2 r, \tag{A4}$$

$$c_3 = \frac{\operatorname{sech}^2 r}{p_S} \eta_t \eta_r T^2 \tanh^2 r, \tag{A5}$$

$$c_4 = \frac{\operatorname{sech}^2 r}{p_S} \eta_t \eta_r R^2 \tanh^2 r, \tag{A6}$$

$$c_5 = \frac{\operatorname{sech}^2 r}{p_S} RT \eta_t \tanh r. \tag{A7}$$

Making partial transpose for mode b, we have

$$\left(\rho_{\rm out}^{S}\right)^{T_b} = \begin{pmatrix} c_1 & 0 & 0 & 0 \\ 0 & c_4 & -c_5 & 0 \\ 0 & -c_5 & c_3 & 0 \\ 0 & 0 & 0 & c_2 \end{pmatrix} = \left[\left(\rho_{\rm out}^{S}\right)^{T_b}\right]^{\dagger}. \tag{A8}$$

The eigenvalues λ_i of partial transpose density operator $(\rho_{\rm out}^{S})^{T_b}$ can be calculated as

$$\lambda_1 = c_1, \quad \lambda_2 = c_2, \tag{A9}$$

$$\lambda_3 = \tfrac{1}{2}c_{3+4} - \tfrac{1}{2}\sqrt{c_{3-4}^2 + 4c_5^2}, \tag{A10}$$

$$\lambda_4 = \tfrac{1}{2}c_{3+4} + \tfrac{1}{2}\sqrt{c_{3-4}^2 + 4c_5^2}, \tag{A11}$$

where $c_{3+4} = c_3 + c_4$, $c_{3-4} = c_3 - c_4$.Thus the degree of entanglement is given by

$$\begin{aligned} E_\rho &= \log_2 \left\| \left(\rho_{\rm out}^{S}\right)^{T_b} \right\|_1 \\ &= \log_2 \mathtt{Tr}\sqrt{\left[\left(\rho_{\rm out}^{S}\right)^{T_b}\right]^2} \\ &= \log_2 \left(\sum_{i=1}^{4} |\lambda_i|\right), \end{aligned} \tag{A12}$$

where $\lambda_1 = R^2(1 + \eta_r^2 \tanh^2 r)/\bar{p}_S$, $\lambda_2 = T^2\eta_t^2 \tanh^2 r/\bar{p}_S$, and

$$\begin{aligned} \lambda_3 &= \frac{1}{2\bar{p}_S}(Q - \sqrt{K})\eta_t \tanh r, \\ \lambda_4 &= \frac{1}{2\bar{p}_S}(Q + \sqrt{K})\eta_t \tanh r, \\ K &= 4T^2R^2 + [(T^2 - R^2)\eta_r \tanh r]^2, \\ Q &= (T^2 + R^2)\eta_r \tanh r, \\ \bar{p}_S &= R^2 + (R^2 + \eta_t - 2R\eta_t)\tanh^2 r. \end{aligned} \tag{A13}$$

APPENDIX B: THE DEGREE OF ENTANGLEMENT CORRESPONDING TO EQ. (41)

For this purpose, we rewrite Eq. (41) as the following matrix form:

$$\rho_{\rm out}^{D} = \frac{\operatorname{sech}^2 r}{4p_D} \begin{pmatrix} c_1' & 0 & 0 & c_5' \\ 0 & c_3 & 0 & 0 \\ 0 & 0 & c_3 & 0 \\ c_5' & 0 & 0 & c_2' \end{pmatrix}, \tag{B1}$$

and

$$\left[\rho_{\rm out}^{D}\right]^{T_b} = \frac{\operatorname{sech}^2 r}{4p_D} \begin{pmatrix} c_1' & 0 & 0 & 0 \\ 0 & c_3' & c_5' & 0 \\ 0 & c_5' & c_3' & 0 \\ 0 & 0 & 0 & c_2' \end{pmatrix}, \tag{B2}$$

where $c_1' = R^2(1 + \eta_r^2 \tanh^2 r)$, $c_2' = T^2\eta_t^2 \tanh^2 r$, $c_5' = TR\eta_t\eta_r \tanh r$, and $c_3' = \eta_t\eta_r TR \tanh^2 r$. The eigenvalues of partial transpose density matrix $[\rho_{\rm out}^{D}]^{T_b}$ are given by

$$\lambda_1' = \frac{1}{\bar{p}_d} R^2\left(1 + \eta_r^2 \tanh^2 r\right), \tag{B3}$$

$$\lambda_2' = \frac{1}{\bar{p}_d} T^2 \eta_t^2 \tanh^2 r, \tag{B4}$$

$$\lambda_3' = \frac{1}{\bar{p}_d} TR\eta_t(\eta_r \tanh r - 1)\tanh r, \tag{B5}$$

$$\lambda_4' = \frac{1}{\bar{p}_d} TR\eta_t(\eta_r \tanh r + 1)\tanh r, \tag{B6}$$

$$\bar{p}_d = R^2 + (R + \eta_t - 2R\eta_t)^2 \tanh^2 r. \tag{B7}$$

Thus the degree of entanglement involved in Eq. (41) can be calculated as

$$E_\rho = \log_2 \left(\sum_{i=1}^{4} |\lambda_i'|\right). \tag{B8}$$

APPENDIX C: DERIVATION OF EQ. (49)

After the measurement, the output state can be shown as

$$\begin{aligned}\rho_{\rm out} &= N\mathtt{Tr}_{ac}\left[(1-|0\rangle_{aa}\langle 0|)|0\rangle_{cc}\langle 0|\rho_{\rm out}^{\rm bef}\right]\\ &= N(\rho_{b1}-\rho_{b2}),\end{aligned} \tag{C1}$$

where $\rho_{\rm out}^{\rm bef}$ is the state before the measurements for a and c modes, i.e.,

$$\rho_{\rm out}^{\rm bef} = B_{ac}B_{bc}\rho_a\rho_b|0\rangle_{cc}\langle 0|B_{bc}^{\dagger}B_{ac}^{\dagger}, \tag{C2}$$

and ρ_{b1} and ρ_{b2} are defined as

$$\rho_{b1} = \mathtt{Tr}_a[{}_c\langle 0|\rho_{\rm out}^{\rm bef}|0\rangle_c] = \mathtt{Tr}_a[\widehat{O}_{ab}\rho_a\rho_b\widehat{O}_{ab}^{\dagger}], \tag{C3}$$

$$\rho_{b2} = {}_{ac}\langle 00|\rho_{\rm out}^{\rm bef}|00\rangle_{ac} = \widehat{P}_{ab}\rho_a\rho_b\widehat{P}_{ab}^{\dagger}, \tag{C4}$$

and

$$\widehat{O}_{ab} \equiv {}_c\langle 0|B_{ac}B_{bc}|0\rangle_c, \quad \widehat{P}_{ab} \equiv {}_{ac}\langle 00|B_{ac}B_{bc}|0\rangle_c. \tag{C5}$$

Next, we solve the operators $\widehat{O}_{ab}$ and $\widehat{P}_{ab}$. For this purpose, we appeal to the normal ordering form of the beam splitter [44], i.e.,

$$B_{ac} =: e^{(\sqrt{T_{ac}}-1)\left(a^{\dagger}a+c^{\dagger}c\right)+(a^{\dagger}c-ac^{\dagger})\sqrt{R_{ac}}}:, \tag{C6}$$

$$B_{bc} =: e^{(\sqrt{T_{bc}}-1)\left(b^{\dagger}b+c^{\dagger}c\right)+(b^{\dagger}c-bc^{\dagger})\sqrt{R_{bc}}}:, \tag{C7}$$

and noticing that ${}_{ac}\langle 00|B_{ac} = {}_{ac}\langle 00|$, thus we see

$$\begin{aligned}\widehat{P}_{ab} &= {}_c\langle 0|B_{bc}|0\rangle_c\,{}_a\langle 0|\\ &=: \exp[(\sqrt{T_{bc}}-1)b^{\dagger}b]:\,{}_a\langle 0|\\ &= (\sqrt{T_{bc}})^{b^{\dagger}b}\,{}_a\langle 0|,\end{aligned} \tag{C8}$$

and

$$\begin{aligned}\widehat{O}_{abab} &= {}_c\langle 0|B_{ac}B_{bc}|0\rangle_c\\ &= {}_c\langle 0|:e^{(\sqrt{T_{ac}}-1)a^{\dagger}a+a^{\dagger}c\sqrt{R_{ac}}}:\\ &\quad\times:e^{(\sqrt{T_{bc}}-1)b^{\dagger}b-bc^{\dagger}\sqrt{R_{bc}}}:|0\rangle_c\\ &=: e^{(\sqrt{T_{ac}}-1)a^{\dagger}a+(\sqrt{T_{bc}}-1)b^{\dagger}b-a^{\dagger}b\sqrt{R_{ac}R_{bc}}}:\\ &= e^{-\sqrt{R_{ac}R_{bc}/T_{bc}}a^{\dagger}b}T_{ac}^{a^{\dagger}a/2}T_{bc}^{b^{\dagger}b/2},\end{aligned} \tag{C9}$$

where we have used the following formula: $e^Ae^B = e^Be^Ae^{[A,B]}$, which is valid for $[A,[A,B]] = [B,[A,B]] = 0$, and the operator identity

$$\begin{aligned}e^{\lambda b^{\dagger}b}be^{-\lambda b^{\dagger}b} &= e^{-\lambda}b,\\ :\exp\{(e^u-1)b^{\dagger}b\}: &= e^{ub^{\dagger}b}.\end{aligned} \tag{C10}$$

Now, we take $\rho_b = [(1+\bar{n})\rho_{th}(\bar{n}) - |0\rangle_{bb}\langle 0|]/\bar{n}$ into account. Using Eq. (C8), Eq. (C4) becomes

$$\begin{aligned}\rho_{b2} &= \widehat{P}_{ab}\rho_a\rho_b\widehat{P}_{ab}^{\dagger}\\ &= \frac{1}{\bar{n}}[(1+\bar{n})\widehat{P}_{ab}\rho_a\rho_{th}(\bar{n})\widehat{P}_{ab}^{\dagger} - \widehat{P}_{ab}\rho_a|0\rangle_{bb}\langle 0|\widehat{P}_{ab}^{\dagger}]\\ &= \frac{1}{\bar{n}}\,{}_a\langle 0|\rho_a|0\rangle_a[(1+\bar{n})\digamma_b - |0\rangle_{bb}\langle 0|],\end{aligned} \tag{C11}$$

where $\digamma_b$ is defined by

$$\digamma_b = (T_{bc})^{b^{\dagger}b/2}\rho_{th}(\bar{n})(T_{bc})^{b^{\dagger}b/2}. \tag{C12}$$

Further using the integration form in coherent-state representation and the normal ordering form of the thermal state [45,46], i.e.,

$$\rho_{th}(\bar{n}) = \frac{1}{\bar{n}}\int\frac{d^2\alpha}{\pi}e^{-\frac{|\alpha|^2}{\bar{n}}}|\alpha\rangle_{bb}\langle\alpha| \tag{C13}$$

$$= \frac{1}{\bar{n}+1}:\exp\left\{-\frac{b^{\dagger}b}{\bar{n}+1}\right\}:, \tag{C14}$$

and the formula

$$g^{b^{\dagger}b}|\alpha\rangle = \exp\left\{\tfrac{1}{2}(g^2-1)|\alpha|^2\right\}|g\alpha\rangle, \tag{C15}$$

as well as

$$\int\frac{d^2\alpha}{\pi}e^{-\xi|\alpha|^2+\eta\alpha+\lambda\alpha^*} = \frac{1}{\xi}e^{\frac{\eta\lambda}{\xi}}, \tag{C16}$$

we have

$$\begin{aligned}\digamma_b &= \int\frac{d^2\alpha}{\bar{n}\pi}e^{-\frac{|\alpha|^2}{\bar{n}}}(T_{bc})^{b^{\dagger}b/2}|\alpha\rangle\langle\alpha|(T_{bc})^{b^{\dagger}b/2}\\ &= \int\frac{d^2\alpha}{\bar{n}\pi}e^{-\frac{|\alpha|^2}{\bar{n}}}e^{(T_{bc}-1)|\alpha|^2}|\sqrt{T_{bc}}\alpha\rangle\langle\sqrt{T_{bc}}\alpha|\\ &= \int\frac{d^2\alpha}{\bar{n}\pi}:e^{-\frac{1+\bar{n}}{\bar{n}}|\alpha|^2+\sqrt{T_{bc}}b^{\dagger}\alpha+\sqrt{T_{bc}}\alpha^*b-b^{\dagger}b}:\\ &= \frac{1}{1+\bar{n}}:\exp\left\{-\frac{\bar{n}R_{bc}+1}{1+\bar{n}}b^{\dagger}b\right\}:\\ &= \frac{x}{\bar{n}T_{bc}}\rho_{th}(x),\end{aligned} \tag{C17}$$

where $x = \bar{n}T_{bc}/(\bar{n}R_{bc}+1)$. In the above derivation of Eq. (C17), the technique of integration within an ordered product (IWOP) of operators is used [47]. Thus, ρ_{b2} is

$$\rho_{b2} = {}_a\langle 0|\rho_a|0\rangle_a\,\Lambda_b = \mathtt{Tr}_a[|0\rangle_{aa}\langle 0|\Lambda_b\rho_a], \tag{C18}$$

where the operator Λ_b is defined in Eq. (51).

Using Eqs. (C9) and (47), Eq. (C3) becomes

$$\begin{aligned}\rho_{b1} &= \frac{1}{\bar{n}}\mathtt{Tr}_a\{(\bar{n}+1)\widehat{O}_{ab}\rho_a\rho_{th}(\bar{n})\widehat{O}_{ab}^{\dagger} - \widehat{O}_{ab}|0\rangle_b\rho_{ab}\langle 0|\widehat{O}_{ab}^{\dagger}\}\\ &= \frac{1}{\bar{n}}[(\bar{n}+1)\mathtt{Tr}_a(\Omega\rho_a) - \mathtt{Tr}_a(T_{ac}^{a^{\dagger}a}\rho_a|0\rangle_{bb}\langle 0|)],\end{aligned} \tag{C19}$$

where

$$\mathtt{Tr}_a[\Omega\rho_a] = \mathtt{Tr}_a[\widehat{O}_{ab}\rho_a\rho_{th}(\bar{n})\widehat{O}_{ab}^{\dagger}]. \tag{C20}$$

Using Eqs. (C13), (C15), and (C16), as well as the IWOP technique again, we can finally obtain

$$\Omega = A_1:e^{-[A_2a^{\dagger}a+A_3b^{\dagger}b+A_4(a^{\dagger}b+b^{\dagger}a)]}:, \tag{C21}$$

where we have defined

$$A_1 = \frac{1}{1+\bar{n}(1-R_{ac}R_{bc})}, \tag{C22}$$

$$A_2 = \frac{(\bar{n}T_{bc}+1)R_{ac}}{1+\bar{n}(1-R_{ac}R_{bc})}, \tag{C23}$$

$$A_3 = \frac{1+\bar{n}R_{bc}T_{ac}}{1+\bar{n}(1-R_{ac}R_{bc})}, \tag{C24}$$

$$A_4 = \frac{\bar{n}\sqrt{T_{ac}T_{bc}R_{ac}R_{bc}}}{1+\bar{n}(1-R_{ac}R_{bc})}. \tag{C25}$$

Thus, Eq. (C19) can be rewritten as

$$\rho_{b1} = \mathrm{Tr}_a[\Lambda_{ab}\rho_a], \tag{C26}$$

$$\Lambda_{ab} = \frac{1}{\bar{n}}[(\bar{n}+1)\Omega - (T_{ac})^{a^\dagger a}|0\rangle_{bb}\langle 0|]. \tag{C27}$$

Combining Eqs. (C18) and (C26) leads to Eq. (49), i.e.,

$$\rho_{\mathrm{out}} = N\mathrm{Tr}_a[(\Lambda_{ab} - \Lambda_b|0\rangle_{aa}\langle 0|)\rho_a]. \tag{C28}$$

APPENDIX D: DERIVATION OF EQ. (55)

Here we consider the TMSV going through a photon-loss channel as inputs shown in Eq. (27). In order to derive the density operator after the single-side quantum scissors device, we only need to calculate three items, as follows. Here, the normal ordering forms in Eqs. (27) and (C14) will be convenient for the following calculations. The first item is

$$\begin{aligned} {}_a\langle 0|\rho_{aa'}|0\rangle_a &= C_1 : e^{-C_2 a'^\dagger a'} : \\ &= \frac{\mathrm{sech}^2 r}{1-\eta_r \tanh^2 r}\rho_{th,a'}(y), \end{aligned} \tag{D1}$$

where $\rho_{th,a'}(y)$ is the thermal state for mode a' with the average photon number $y = \eta_t\eta_r \tanh^2 r/(1-\eta_r \tanh^2 r) > 0$. The second item is

$$\begin{aligned} &\mathrm{Tr}_a[(T_{ac})^{a^\dagger a}\rho_{aa'}] \\ &= C_1\mathrm{Tr}_a[T_{ac}^{a^\dagger a} : e^{-C_2(a^\dagger a + a'^\dagger a') + C_3(a^\dagger a'^\dagger + aa')} :]. \end{aligned} \tag{D2}$$

In order to get the normal ordering form of Eq. (D2), using the completeness of the coherent state and the IWOP technique, as well as noticing that

$$\begin{aligned} (T_{ac})^{a^\dagger a} &= (T_{ac})^{a^\dagger a/2}\int_{-\infty}^{\infty}\frac{d^2\alpha}{\pi}|\alpha\rangle_{aa}\langle\alpha|(T_{ac})^{a^\dagger a/2} \\ &= \int_{-\infty}^{\infty}\frac{d^2\alpha}{\pi}e^{-R_{ac}|\alpha|^2}|\sqrt{T_{ac}}\alpha\rangle_{aa}\langle\sqrt{T_{ac}}\alpha|, \end{aligned} \tag{D3}$$

we have

$$\begin{aligned} &\mathrm{Tr}_a[(T_{ac})^{a^\dagger a}\rho_{aa'}] \\ &= C_1\int_{-\infty}^{\infty}\frac{d^2\alpha}{\pi}e_a^{-R_{ac}|\alpha|^2}\langle\sqrt{T_{ac}}\alpha| \\ &\quad\times : e^{-C_2(a^\dagger a + a'^\dagger a') + C_3(a^\dagger a'^\dagger + aa')} : |\sqrt{T_{ac}}\alpha\rangle_a \\ &= \frac{\mathrm{sech}^2 r}{1-(\eta_r+\eta_t T_{ac})\tanh^2 r}\rho_{th,a'}(z), \end{aligned} \tag{D4}$$

with

$$z = \frac{\eta_t(\eta_r+\eta_t T_{ac})\tanh^2 r}{1-(\eta_r+\eta_t T_{ac})\tanh^2 r}. \tag{D5}$$

The last item is $\mathrm{Tr}_a(\Omega\rho_{aa'})$, which can be calculated in a similar way to deriving Eq. (D4). Using the completeness of two coherent states and the IWOP technique, we finally obtain

$$\begin{aligned} \mathrm{Tr}_a(\Omega\rho_{aa'}) &= C_1\int_{-\infty}^{\infty}\frac{d^2\alpha d^2\beta}{\pi^2}{}_a\langle\alpha|\,\Omega\,|\beta\rangle_a \\ &\quad\times {}_a\langle\beta| : e^{-C_2(a^\dagger a + a'^\dagger a') + C_3(a^\dagger a'^\dagger + aa')} : |\alpha\rangle_a \\ &= W_1 : e^{-W_2 a'^\dagger a' - W_3 b^\dagger b - W_4(a'b + a'^\dagger b^\dagger)} :, \end{aligned} \tag{D6}$$

where we have defined

$$W_1 = \frac{A_1 C_1}{A_2 + (1-A_2)C_2}, \tag{D7}$$

$$W_2 = \frac{(1-A_2)\left(C_2^2 - C_3^2\right) + A_2 C_2}{A_2 + (1-A_2)C_2}, \tag{D8}$$

$$W_3 = \frac{(1-C_2)\left(A_2 A_3 - A_4^2\right) + A_3 C_2}{A_2 + (1-A_2)C_2}, \tag{D9}$$

$$W_4 = \frac{A_4 C_3}{A_2 + (1-A_2)C_2}. \tag{D10}$$

Then, substituting Eqs. (D1), (D4), and (D6) into Eq. (49), we can see that

$$\mathrm{Tr}_a(\Lambda_{ab}\rho_{aa'}) = \widehat{O} - P_1\rho_{th,a'}(z)|0\rangle_{bb}\langle 0|, \tag{D11}$$

and

$$\mathrm{Tr}_a[\Lambda_b|0\rangle_{aa}\langle 0|\rho_{aa'}] = [P_2\rho_{th}(x) - P_3|0\rangle_{bb}\langle 0|]\rho_{th,a'}(y), \tag{D12}$$

where we have set

$$\widehat{O} = \frac{\bar{n}+1}{\bar{n}}W_1 : e^{-W_2 a'^\dagger a' - W_3 b^\dagger b - W_4(a'b + a'^\dagger b^\dagger)} :, \tag{D13}$$

$$P_1 = \frac{1}{\bar{n}}\frac{\mathrm{sech}^2 r}{1-(\eta_r+\eta_t T_{ac})\tanh^2 r}, \tag{D14}$$

$$P_2 = \frac{\bar{n}+1}{\bar{n}}\frac{\mathrm{sech}^2 r}{1-\eta_r\tanh^2 r}\frac{x}{\bar{n}T_{bc}}, \tag{D15}$$

$$P_3 = \frac{1}{\bar{n}}\frac{\mathrm{sech}^2 r}{1-\eta_r\tanh^2 r}. \tag{D16}$$

Thus, the final output state is given by

$$\begin{aligned} \rho_{\mathrm{out}}^S &= N\mathrm{Tr}_a[(\Lambda_{ab} - \Lambda_b|0\rangle_{aa}\langle 0|)\rho_{aa'}] \\ &= N\{\widehat{O} - P_2\rho_{th,a'}(y)\rho_{th}(x) \\ &\quad + [P_3\rho_{th,a'}(y) - P_1\rho_{th,a'}(z)]|0\rangle_{bb}\langle 0|\}, \end{aligned} \tag{D17}$$

and the normalized factor is

$$N^{-1} = \mathrm{Tr}(\hat{O}) + P_3 - P_1 - P_2, \tag{D18}$$

where $\mathrm{Tr}(\widehat{O})$ can be given from Eq. (D13), i.e.,

$$\mathrm{Tr}(\widehat{O}) = \frac{\bar{n}+1}{\bar{n}}\frac{W_1}{W_2 W_3 - W_4^2}. \tag{D19}$$

[1] D. Bouwmeester, A. Ekert, and A. Zeilinger, *The Physics of Quantum Information* (Springer-Verlag, Berlin, 2000).

[2] S. L. Braunstein and P. van Loock, Quantum information with continuous variables, Rev. Mod. Phys. **77**, 513 (2005).

[3] J. Eisert, S. Scheel, and M. B. Plenio, Distilling Gaussian States with Gaussian Operations is Impossible, Phys. Rev. Lett. **89**, 137903 (2002).

[4] G. Giedke and J. I. Cirac, Characterization of Gaussian operations and distillation of Gaussian states, Phys. Rev. A **66**, 032316 (2002).

[5] J. Fiurasek, Gaussian Transformations and Distillation of Entangled Gaussian States, Phys. Rev. Lett. **89**, 137904 (2002).

[6] A. Zavatta, S. Viciani, and M. Bellini, Quantum-to classical transition with single-photon-added coherent states of light, Science **306**, 660 (2004).

[7] G. S. Agarwal and K. Tara, Nonclassical properties of states generated by the excitations on a coherent state, Phys. Rev. A **43**, 492 (1991).

[8] A. Kitagawa, M. Takeoka, M. Sasaki, and A. Chefles, Entanglement evaluation of non-Gaussian states generated by photon subtraction from squeezed states, Phys. Rev. A **73**, 042310 (2006).

[9] A. Ourjoumtsev, A. Dantan, R. Tualle-Brouri, and Ph. Grangier, Increasing Entanglement between Gaussian States by Coherent Photon Subtraction, Phys. Rev. Lett. **98**, 030502 (2007).

[10] L.-Y. Hu, X.-X. Xu, Z.-S. Wang, and X.-F. Xu, Photon-subtracted squeezed thermal state: Nonclassicality and decoherence, Phys. Rev. A **82**, 043842 (2010).

[11] S. Y. Lee and H. Nha, Quantum state engineering by a coherent superposition of photon subtraction and addition, Phys. Rev. A **82**, 053812 (2010).

[12] J. Fiurasek, Distillation and purification of symmetric entangled Gaussian states, Phys. Rev. A **82**, 042331 (2010).

[13] S. L. Zhang and P. van Loock, Distillation of mixed-state continuous-variable entanglement by photon subtraction, Phys. Rev. A **82**, 062316 (2010).

[14] J. Fiurasek, Improving entanglement concentration of Gaussian states by local displacements, Phys. Rev. A **84**, 012335 (2011).

[15] J. N. Wu, S. Y. Liu, L. Y. Hu, J. H. Huang, Z. L. Duan, and Y. H. Ji, Improving entanglement of even entangled coherent states by a coherent superposition of photon subtraction and addition, J. Opt. Soc. Am. B **32**, 2299 (2015).

[16] A. Datta, L. Zhang, J. Nunn, N. K. Langford, A. Feito, M. B. Plenio, and I. A. Walmsley, Compact Continuous-Variable Entanglement Distillation, Phys. Rev. Lett. **108**, 060502 (2012).

[17] Y. Kurochkin, A. S. Prasad, and A. I. Lvovsky, Distillation of The Two-Mode Squeezed State, Phys. Rev. Lett. **112**, 070402 (2014).

[18] T. J. Bartley, P. J. D. Crowley, A. Datta, J. Nunn, L. Zhang, and I. Walmsley, Strategies for enhancing quantum entanglement by local photon subtraction, Phys. Rev. A **87**, 022313 (2013).

[19] A. I. Lvovsky and J. Mlynek, Quantum-Optical Catalysis: Generating Nonclassical States of Light by Means of Linear Optics, Phys. Rev. Lett. **88**, 250401 (2002).

[20] L. Y. Hu, Z. Y. Liao, and M. S. Zubairy, Continuous-variable entanglement via multiphoton catalysis, Phys. Rev. A **95**, 012310 (2017).

[21] T. J. Bartley and I. A. Walmsley, Directly comparing entanglement-enhancing non-Gaussian operations, New J. Phys. **17**, 023038 (2015).

[22] S. L. Zhang, J. S. Guo, W. S. Bao, J. H. Shi, C. H. Jin, X. B. Zou, and G. C. Guo, Quantum illumination with photon-subtracted continuous-variable entanglement, Phys. Rev. A **89**, 062309 (2014).

[23] L. Fan and M. S. Zubairy, Quantum illumination using non-Gaussian states generated by photon subtraction and photon addition, Phys. Rev. A **98**, 012319 (2018).

[24] S. Kocsis, G. Y. Xiang, T. C. Ralph and G. J. Pryde, Heralded noiseless amplification of a photon polarization qubit, Nat. Phys. **9**, 23 (2013).

[25] H. M. Chrzanowski, N. Walk, S. M. Assad, J. Janousek, S. Hosseini, T. C. Ralph, T. Symul, and P. K. Lam, Measurement-based noiseless linear amplification for quantum communication, Nat. Photon. **8**, 333 (2014).

[26] T. C. Ralph and A. P. Lund, Nondeterministeric niosless linear amplification of quantum systems, in *Quantum Communication, Measurement and Computing (QCMC): Ninth International Conference on QCMC*, AIP Conf. Proc. No. 1110 (AIP, New York, 2009), p. 155.

[27] D. T. Pegg, L. S. Phillips, and S. M. Barnett, Optical State Truncation by Projection Synthesis, Phys. Rev. Lett. **81**, 1604 (1998).

[28] G. Y. Xiang, T. C. Ralph, A. P. Lund, N. Walk, and G. J. Pryde, Heralded noiseless linear amplification and distillation of entanglement, Nat. Photon. **4**, 316 (2010).

[29] S. Zhang and X. Zhang, Photon catalysis acting as noiseless linear amplification and its application in coherence enhancement, Phys. Rev. A **97**, 043830 (2018).

[30] Y. Guo, W. Ye, H. Zhong, and Q. Liao, Continuous-variable quantum key distribution with non-Gaussian quantum catalysis, Phys. Rev. A **99**, 032327 (2019).

[31] F. Ferreyrol, M. Barbieri, R. Blandino, S. Fossier, R. Tualle-Brouri, and P. Grangier, Implementation of a Nondeterministic Optical Noiseless Amplifier, Phys. Rev. Lett. **104**, 123603 (2010).

[32] M. O. Scully and M. S. Zubairy, *Quantum Optics* (Cambridge University Press, New York, 1997).

[33] G. Vidal and R. F. Werner, Computable measure of entanglement, Phys. Rev. A **65**, 032314 (2002).

[34] M. B. Plenio and S. Virmani, An introduction to entanglement measures, Quantum Inf. Comput. **7**, 1 (2007) and references therein.

[35] L. Y. Hu, F. Chen, Z. S. Wang, and H. Y. Fan, Time evolution of distribution functions in dissipative environments, Chin. Phys. B **20**, 074204 (2011).

[36] D. Gottesman, A. Kitaev, and J. Preskill, Encoding a qubit in an oscillator, Phys. Rev. A **64**, 012310 (2001).

[37] H. Y. Fan and H. R. Zaidi, Application of IWOP technique to the generalized Weyl correspondence, Phys. Lett. A **124**, 303 (1987).

[38] C. Navarrete-Benlloch, R. Garcia-Patron, J. H. Shapiro, and N. J. Cerf, Enhancing quantum entanglement by photon addition and subtraction, Phys. Rev. A **86**, 012328 (2012).

[39] H. L. Zhang, Y. Q. Hu, F. Jia, and L. Y. Hu, Entanglement of Photon-Subtracted Two-Mode Squeezed Thermal State and Its Decoherence in Thermal Environments, Int. J. Theor. Phys. **53**, 2091 (2014).

[40] P. Huang, G. He, J. Fang, and G. Zeng, Performance improvement of continuous-variable quantum key distribution via photon subtraction, Phys. Rev. A **87**, 012317 (2013).

[41] D. Wang, M. Li, F. Zhu, Z. Q. Yin, W. Chen, Z. F. Han, G. C. Guo, and Q. Wang, Quantum key distribution with the single-photon-added coherent source, Phys. Rev. A **90**, 062315 (2014).

[42] Z. Li, Y. Zhang, X. Wang, B. Xu, X. Peng, and H. Guo, Non-Gaussian postselection and virtual photon subtraction in continuous-avarible quantum key distribution, Phys. Rev. A **93**, 012310 (2016).

[43] S. W. Ji, J. Lee, J. Park, and H. Nha, Quantum steering of Gaussian states via non-Gaussian measurements, Sci. Rep. **6**, 29729 (2016).

[44] F. Jia, X. X. Xu, C. J. Liu, J. H. Huang, L. Y. Hu, and H. Y. Fan, Decompositions of beam splitter operator and its entanglement function, Acta Phys. Sin. **63**, 220301 (2014).

[45] S. M. Barnett and P. M. Radmore, *Methods in Theoretical Quantum Optics* (Clarendon Press, Oxford, 1997).

[46] L. Y. Hu, H. Y. Fan, and Z. M. Zhang, New formulas for normalizing photon-added (-subtracted) two-mode squeezed thermal states, Chin. Phys. B **22**, 034202 (2013).

[47] H. Y. Fan, H. L. Lu, and Y. Fan, Newton-Leibniz integration for ket-bra operators in quantum mechanics and derivation of entangled state representations, Ann. Phys. **321**, 480 (2006).